Discrete homogenization of architectured materials: Implementation of the method in a simulation tool for the systematic prediction of their effective elastic properties

F. Dos Reis, J.F. Ganghoffer

The kinematics and the balance equations for multiphase micro-architectured materials such as foams, textiles, or beam-like structures exhibit a peculiar macroscopic behavior. The topology and mechanical properties of their structural constituents at the microscale induce this behavior. The derivation of the effective mechanical properties of 2D and 3D lattices made of articulated beams is herewith investigated. The asymptotic homogenization technique is used to get closed form expressions of the equivalent properties versus the geometrical and mechanical micro-parameters. The effective behavior of a 2D hexagonal lattice is calculated, and is validated by comparison with FE simulations results. In order to analyze the respective roles of flexion and extension at both the micro and macro scales, a mixed lattice has been conceived, accounting for both extensional and flexional effects in a versatile manner. Its effective moduli are calculated versus geometrical and mechanical parameters of the beams. The scaling law of the effective traction modulus versus density shows a complex nonlinear evolution. This law has a drastic decrease when flexional modes become dominant over extensional ones. The obtained compliance matrix does not exhibit the expected symmetries when shear behavior is considered, which is explained by the too restrictive assumption of rotations being suppressed at the edges. After extending the present methodology towards the 3D case, the effective mechanical behavior of Kelvin foams under compression is obtained with an isotropic continuum behavior which is in good agreement with both the literature and FE simulations. The effective compliance matrix of the equivalent continuum does not exhibit some of the required material symmetries under shear when the edge node rotations are prevented. A classification of lattices with respect to the choice of the equivalent continuum model is proposed, according to the nature of the boundary conditions, considering especially boundary micro-rotations. One of the main results of the present contribution is the need for an extension of the asymptotic homogenization to a micro-polar continuum, by considering lattice micro-rotations as additional degrees of freedom at the microscopic and macroscopic scale.

1 Introduction

Architectured materials such as polymeric and metallic foams as well as network models (biological membranes) have attracted the interest of many researchers in the last decade. This is due to their specific mechanical properties, which make them suitable materials for their high crash absorbing capacity. The derivation of the mechanical properties of foams with a regular architecture (in the sense of being endowed with a quasi periodic network), in relation to the topology of the cellular material and the material mechanical properties, is especially interesting and important. It allows for understanding the mechanical behavior, and the foam architecture required to achieve optimized properties at the structural level. The appropriate size materials, the lattice topology and mechanical properties can be selected based on a quantitative understanding of the macroscopic impact of the microstructural parameters.

Attempts to derive those effective properties as closed form expressions of the geometrical and mechanical parameters of the lattice representing the foam are so far not satisfactory. This may be attributed to the difficulty of the task when considering the association of complex geometries and multi-axial loadings. However, this complexity is essential to reproduce the behavior of foams and lattices during their service life. The role of imperfections and heterogeneities, like strain localization phenomena (accompanied by density heterogeneities) as well as the need to extend the kinematics (extra nodal degrees of freedom, such as microrotation), may also prevent or complicate this task.

Accordingly there is clearly a need to develop a general and versatile tool able to calculate the effective behavior

of architectured materials endowed with a discrete topology, in a systematic and automatic manner.

A brief summary of the main literature works is next exposed. Zhang and Lu (2007) study the nonlinear behavior of foams under strong compression, and performed a numerical study for a lattice modified by a Voronoi type perturbation. In the same spirit, Li et al. (2006) analyzes the effects of mesh imperfections, using an energetic averaging on a RVE; see also Burgardt and Cartraud (1999) in the line of energetic averaging method with a periodic lattice. One can also mention in the same line of thoughts the contribution of Badiche et al. (2000), whereby the authors use a quasi periodical model to describe the non uniformity of stresses generated in a truss under strong compressive loads in the plastic regime. In Sullivan et al. (2008), the authors develop a micro-mechanical model based on an energetic approach; the model accounts for the eventual anisotropy induced by the lattice deformation along an axis, which accounts for the observed increase of length of certain foams due to the fabrication process. Nevertheless, all the aforementioned references, including the fundamental work by Zhu et al. (1997) on the tetrakaidecahedral truss, reflect a case by case approach in the sense Zhu and al. have to adopt assumptions related to the reciprocal deformation of the beams within the lattice. The complexity of the task is reflected by the complexity of the calculations required for each specific considered architecture. A big advantage and superiority of the discrete homogenization technique lies in the automatic calculation of the effective behavior. This technique is solely based upon the geometrical representation of the truss; it allows in most cases (at least in a small displacements and strains framework) to derive closed form expressions of the effective moduli, explicitly reflecting the microscopic geometrical and mechanical parameters at the unit cell level.

In the present contribution, we elaborate a variant of the asymptotic homogenization technique recently developed by (Mourad (2003); Caillerie et al. (2006); Tollenaere and Caillerie (1998); Raoult et al. (2008)) in view of the calculation of the effective behavior of periodic lattices. This methodology is applied to various 2D lattices under compression and shear. In order to validate the effective moduli calculated from the asymptotic homogenization, a series of FE simulations has been performed for the 2D hexagonal truss, in a manner similar to Alkhader and Vural (2008). The principle of those simulations has also been exploited by Roberts and Garboczi (2002). The present results will further be compared with the reference results from Gibson and Ashby (1997), related to foams with flexion as the dominant deformation mode, and relying on an empirical argumentation essentially based on dimensional analysis (Despois et al. (2006)).

As a further motivation, a result announced in Gibson and Ashby relative to the principal deformation mode of beams for hexagonal lattice (with reference to honeycombs) under compression is 'clamped without rotation of the boundaries' (Figure 1); although this assumption is invalid in some loading cases, we adopt it in the present work.

Therefore, we shall primarily focus on loading the trusses considered below in tension / compression. However, we note that the assumption of non-rotating nodes directly influences the choice of the equivalent continuous medium, non-polar in the present work.

We herewith restrict us to kinematics to the linear geometrical framework, which is justified for most of the applications in view (foams and networks in the elastic regime). We further focus on the derivation of the elastic properties of foams, or more generally architectured materials endowed with a discrete and periodic topology at the micro level. The main steps of the discrete homogenization technique are first exposed, highlighting the novelty of the present approach. Derivations of effective mechanical properties are first achieved for 2D geometries, with closed form expressions being compared with FE simulations. The extension to 3D architecture is next envisaged, considering more particularly Kelvin foams, recognized as a prototype architecture of many foams.

2 Effective mechanical behavior of 2D lattices from discrete homogenization

Materials with cellular structure are widespread in nature and include wood, cork, trabecular bone. The microstructural features of cellular solids affecting their mechanical response are most easily observed in engineering honeycombs and foams, Gibson (2005). Metallic and polymeric foams usually do not deform homogeneously under compression or multiaxial loading, and strain localization bands form in compression. The plateau observed on the overall load displacement curve results from the formation and propagation of such bands. The densification starts when all cell rows are crushed. These strain localization phenomena must normally be taken into account for the identification of a constitutive model, as well as the heterogeneous density field, which can be identified from tomography analysis. The typical response of foam under compression exhibits three main stages:

- An elastic phase limited to small deformations;
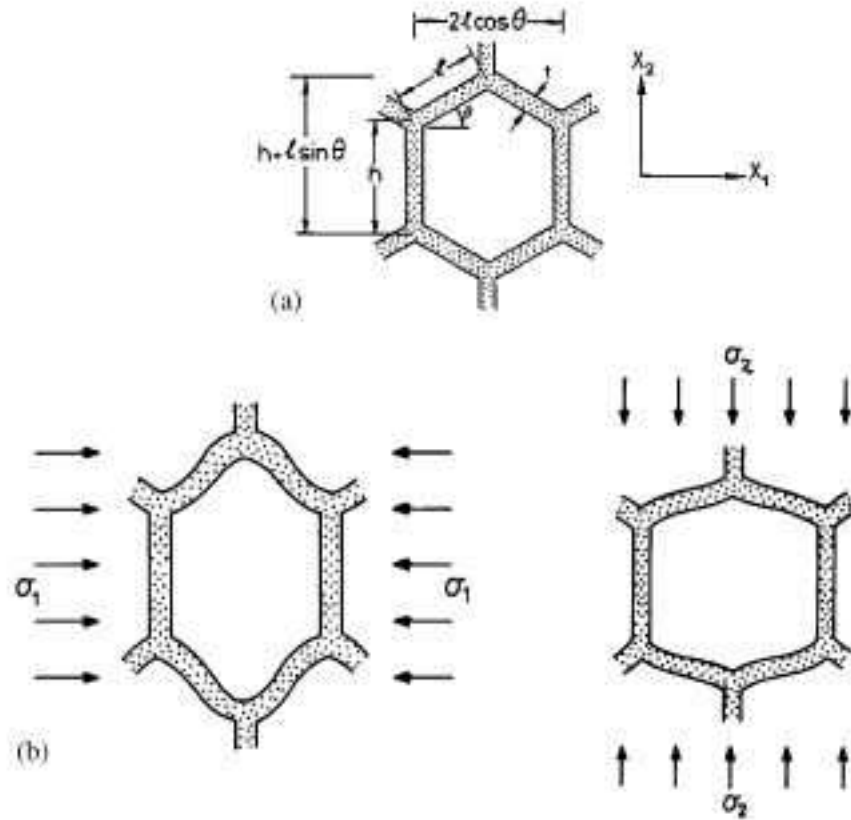
Figure 1: Deformation modes of a honeycomb structure according to Gibson and Ashby (1997)

- A second plateau zone which is beneficial for shock absorption;

- A third phase of densification characterized by a strong increase of the loading.

The cellular architecture and the mechanical properties of the foam material are responsible of these remarkable properties; accordingly, any mechanical analysis of the behavior of foams consists of trying to link the overall properties of foams to their cellular architecture and to the mechanical properties of the underlying constitutive material (Gibson (2005)). The advance in manufacturing technique promises that, in the near future, the fabrication of functional cellular structures will be achieved with the desired cellular microstructure tailored to specific application in mind. In this perspective, it is essential to develop a detailed understanding of the relationship between mechanical response and the cellular microstructure (Alkhader and Vural (2008)).

Here we concentrate on the first deformation stage at low densities, when densification does not yet take place and the overall response may still be modeled as elastic.

2.1 Discrete homogenization: description of the method

Generally speaking, the discrete homogenization can be described as a mathematical method to derive the equivalent continuous medium behavior of a repetitive discrete structure made of elementary cells. This technique is inspired by the homogenization of periodic media developed since the early eighties (Bakhvalov & Panasenko, 1984, Panasenko, 1983, Sanchez, 1980); it has been recently applied by (Mourad (2003)), (Warren and Byskov (2002)). More recently, (Pradel and Sab (1998)) applied the discrete homogenization in combination with the energy method. The general idea at the base of the method is the periodic repetition of an elementary cell made of beams connected at nodes to define an infinite lattice; it may explained as follows. Consider a finite 2D (surface) or 3D structure, parametrized by a small parameter, the ratio between a characteristic length of the basic cell length to a characteristic length of the structure. Maintaining the reference area or volume fixed, one considers the limit situation of a continuous density of unit cells obtained when the small parameter tends to zero. In this limit, a continuum, equivalent in a certain sense to the initial lattice, is obtained. To obtain this limit behavior, one

does mathematically study the equilibrium of the lattice and the dependence of is governing equations versus the introduced small parameter. Asymptotic expansions of the nodal position, tensions and external forces are written and inserted in the equilibrium equations, preferably expressed in weak form. Taylor series expansion of the displacements and possibly rotational degrees of freedom are next inserted into these equilibrium equations. The discrete sums are finally converted in the limit of a continuous density of beams into Riemann integrals, thereby highlighting continuous stress and strain measures. We refer the reader to papers by Caillerie and Tolleneare regarding the more mathematical aspects and the implementation of the method, however restricting to lattices of articulated beams Mourad (2003); Caillerie et al. (2006); Tollenaere and Caillerie (1998); Raoult et al. (2008). The focus in the present paper is on the geometrical linear framework (the beam orientation and length are supposed fixed), which will prove sufficient for the applications in view. The writing of the equivalent continuum behavior allows next to identify the equivalent properties (traction and shear moduli, Poisson's coefficient, density) of the homogenized lattice versus the lattice geometrical and mechanical properties.

The forthcoming sections will expose in a synthetic manner the principal steps of the discrete homogenization technique, as a variant of the method originally developed in (Mourad (2003); Caillerie et al. (2006); Tollenaere and Caillerie (1998); Raoult et al. (2008)). The essential modification brought to the methodology developed by previous authors is the the consideration of beam lattices, wich entails a specific definition adopted for the transverse force; this technical point will be developed in the paragraph 2.1.4.

2.1.1 First step: formulation of the equilibrium involving the stress vector $\mathbf{S^i}$

To simplify subsequent technical developments, we assume nil body forces, and choose the virtual velocity field $\mathbf{v}$ such that it vanishes at the edges; hence, the weak form of equilibrium over a domain $\mathbf{\Omega}$ writes in terms of the Cauchy stress σ.

$$\int_\Omega \sigma : \nabla_x \mathbf{v} dx = 0 \tag{1}$$

with ∇_x the gradient with respect to the variable x, the double point denoting the double contraction of two second order tensors. A change of coordinates is performed in order to express the previous equation in a set of curvilinear coordinates $\lambda = (\lambda^1, \lambda^2, \lambda^3)$; we thereby follow the method exposed in Mourad (2003). The spatial position of a material point P is written $\mathbf{x} = x^i \mathbf{e_i}$ in Cartesian coordinates, as an expression of the vector function

$$\mathbf{x} = \mathbf{R}(\lambda^1, \lambda^2, \lambda^3) \tag{2}$$

A covariant basis in curvilinear coordinates can be defined as the set of vectors

$$\mathbf{e_k^\lambda} = \frac{\partial x^i}{\partial \lambda^i} \mathbf{e_i} \tag{3}$$

The contravariant basis vectors of the curvilinear coordinate system, $\mathbf{e}_\lambda^i$, are defined by

$$\mathbf{e_\lambda^i} \cdot \mathbf{e_j^\lambda} = \delta_j^i \tag{4}$$

with δ_j^i the Kronecker symbol. In order to obtain the expression of the stress tensor in generalized curvilinear coordinates, we make the change of variables $x = x(\lambda)$ in the equation (1); the Jacobian of this transformation is g, hence $dx = gd\lambda$. For a virtual velocity field $\mathbf{v}$, this coordinate change induces the following relations between the velocity gradients

$$\nabla_x \mathbf{v} = \frac{\partial \mathbf{v}}{\partial \lambda^i} \otimes \mathbf{e_\lambda^i} \tag{5}$$

The equation (1) can then be expressed in the form

$$\int_\Omega \sigma : (\nabla_x \mathbf{v}) dx = \int_\Omega \sigma : (\frac{\partial \mathbf{v}}{\partial \lambda^i} \otimes \mathbf{e_\lambda^i}) g d\lambda = \int_\Omega (\sigma \cdot \mathbf{e_\lambda^i}) . \frac{\partial \mathbf{v}}{\partial \lambda^i} g d\lambda = 0 \tag{6}$$
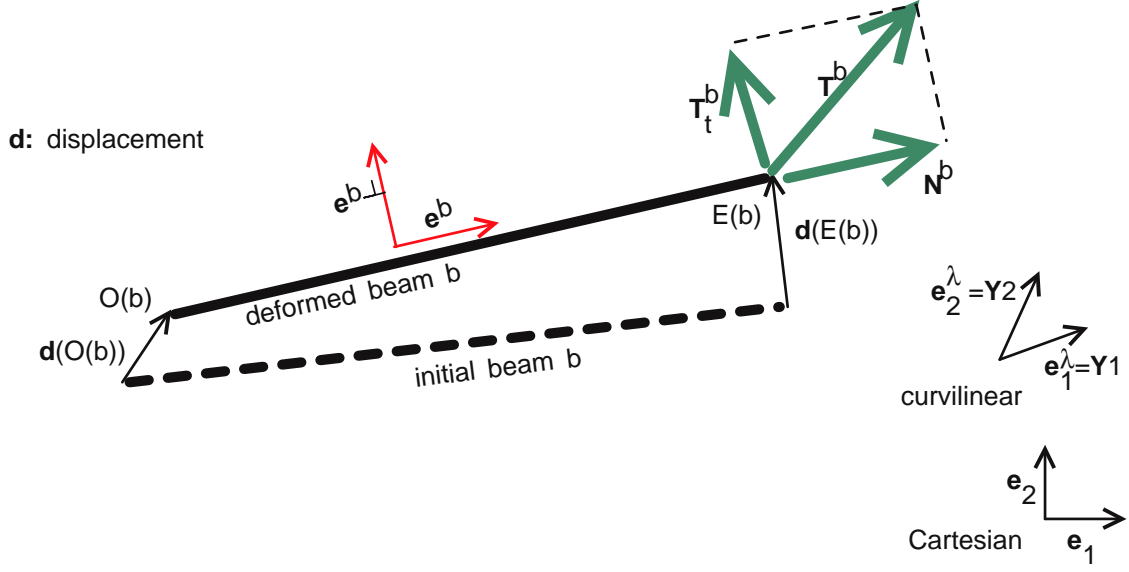
Figure 2: Kinematic and static variables for a beam element

One accordingly sets the stress vector as

$$\mathbf{S^i} = g\sigma \cdot \mathbf{e}^{\mathbf{i}}_\lambda \tag{7}$$

The equilibrium equation follows from the equations (6) and (7) in terms of the stress vector $\mathbf{S^i}$

$$\int_\Omega \mathbf{S^i} \cdot \frac{\partial \mathbf{v}}{\partial \lambda^i} d\lambda = 0 \tag{8}$$

From the definition (7) and the equilibrium equation (6), one can then express the force-stress tensor as the dyadic products of the stress vector $\mathbf{S^i}$ with the position gradient $\dfrac{\partial \mathbf{R}}{\partial \lambda^i}$

$$\sigma = \frac{1}{g}\mathbf{S^i} \otimes \mathbf{e}^\lambda_{\mathbf{i}} = \frac{1}{g}\mathbf{S^i} \otimes \frac{\partial \mathbf{R}}{\partial \lambda^i} \tag{9}$$

We next calculate the stress vector $\mathbf{S^i}$ from the homogenization of the beam's lattice equilibrium equations.

2.1.2 Second step: homogenization of the discrete equilibrium equations

As a prerequisite, we number the nodes and the beams and define a unit direction for these beams. We define the set $\mathcal{B}(\tilde{b})$, composed of beams numbered $\tilde{b}$ and the set of nodes $\mathcal{N}(\tilde{n})$ consisting of nodes numbered $\tilde{n}$. We also define the following three sets of beams $\tilde{b}$, $\mathcal{O}(\tilde{n})$, $\mathcal{E}(\tilde{n})$ et $\mathcal{E}\lceil(\tilde{n})$. In these sets, $\tilde{n}$ is the origin, end or side node respectively. We summarize some of the useful notations in Figure 2.

We denote the force applied to a beam $\tilde{b}$ to the end node $\tilde{n}$ by $\mathbf{T}^{\tilde{b}}$. The balance equilibrium of each beam immediately implies that there is an opposite force $-\mathbf{T}^{\tilde{b}}$ acting on the origin node. The forces at the nodes of edges will be denoted $\mathbf{f}^{\tilde{b}}$. With these notations, one can write the equilibrium equation of the lattice

$$\sum_{\tilde{b}\in\mathcal{O}(\tilde{n})} \mathbf{T}^{\tilde{b}} - \sum_{\tilde{b}\in\mathcal{E}(\tilde{n})} \mathbf{T}^{\tilde{b}} + \sum_{\tilde{b}\in\mathcal{E}\lceil(\tilde{n})} \mathbf{f}^{\tilde{b}} = \mathbf{0} \tag{10}$$

We assume that no rotations occurs at the lattice nodes, and therefore no couple stresses acting on the lattice edges. These assumptions will be further discussed regarding their validity in the sequel. The previous equilibrium

equation (10) is conveniently expressed in virtual power form

$$\sum_{\tilde{b} \in \mathcal{B}(\tilde{b})} \mathbf{T}^{\tilde{b}} \cdot \left[\mathbf{v}\left(O\left(\tilde{b}\right)\right) - \mathbf{v}\left(E\left(\tilde{b}\right)\right) \right] = \mathbf{0} \tag{11}$$

Written in this form, the summation over all the beams is difficult to handle: we will instead rewrite the previous equation by decomposing this sum, changing the way the geometry of the lattice is represented. In order to describe an infinite lattice, we decompose the sets used above, $\mathcal{B}(\tilde{b})$ and $\mathcal{N}(\tilde{n})$ repeating on $\mathbb{Z}^3$ an elementary cell of the lattice, which we call reference cell. We hypothesize that in its deformed state the lattice is quasiperiodic. In the reference cell, the sets of nodes and beams are finite dimensional, and are named $\mathcal{N}_{\mathcal{R}}$ and $\mathcal{B}_{\mathcal{R}}$ respectively. Thus, to any triplet $v^i = (v^1, v^2, v^3) \in \mathbb{Z}^3$ (doublet in 2D), we associate a basic cell; hence, the nodes of the whole lattice can be described by the quadruplets $\tilde{n} = (n, v^1, v^2, v^3)$ in $\mathcal{N}_{\mathcal{R}} \times \mathbb{Z}^3$ and beams of the whole lattice can be described by $\tilde{b} = (b, v^1, v^2, v^3)$ in $\mathcal{B}_{\mathcal{R}} \times \mathbb{Z}^3$.

With these notations, we note that within the reference cell one can select the node of origin of a beam $O(\tilde{b})$ so that it belongs to the reference cell. This origin node can be represented by the quadruplet (n, v^1, v^2, v^3). Nevertheless, the end node $E(\tilde{b})$ does not necessarily belong to the reference cell, but is necessarily included in an adjacent cell numbered by $(v^1 + \delta^1, v^2 + \delta^2, v^3 + \delta^3)$. The triplet $(\delta^1, \delta^2, \delta^3) \in \mathbb{Z}^3$, and the end node either belongs to the reference cell or to a cell next to it: this means that in the general case $\delta^i \in \{-1, 0, 1\}$; these integers δ^i will be particularly useful in the discrete homogenization phase.

At this step, we can rewrite the equation (11) as a double sum

$$\sum_{v^i \in \mathbb{Z}^3} \sum_{b \in \mathcal{B}_R} \mathbf{T}^{\mathbf{b}} \cdot \left[\mathbf{v}\left(O\left(b\right)\right) - \mathbf{v}\left(E\left(b\right)\right) \right] = \mathbf{0} \tag{12}$$

We can decompose $\mathbf{T}^{\mathbf{b}}$ in a normal and a transverse force, hence the principle of virtual power is

$$\sum_{v^i \in \mathbb{Z}^3} \sum_{b \in \mathcal{B}_R} \left(\mathbf{N}^b + \mathbf{T}_t^b \right) \cdot \left[\mathbf{v}\left(O\left(b\right)\right) - \mathbf{v}\left(E\left(b\right)\right) \right] = \mathbf{0} \tag{13}$$

The discrete homogenization, like the periodic media homogenization, is based on asymptotic expansions of the kinematic and static variables versus a small parameter ε, ratio of a typical length characteristic of an elementary cell to a structural length. We consider that this small parameter $\varepsilon \to 0$. To homogenize, it is necessary to parameterize the entire structure by ε; this concerns the geometry as well as the constitutive behavior. We accordingly set the Lagrangian curvilinear coordinates as $\lambda^\varepsilon = \varepsilon v^i$.

The positions of nodes can then be defined by the vectorial function

$$\mathbf{R}^\varepsilon(\tilde{n}) = \mathbf{R}^0(\lambda^\varepsilon) + \varepsilon \mathbf{R}^{n1}(\lambda^\varepsilon) + ... \tag{14}$$

With $\mathbf{R}^0(\lambda^\varepsilon)$ the leading term. We associate a function of the node displacement as

$$\mathbf{d}^\varepsilon(\tilde{n}) = \mathbf{d}^0(\lambda^\varepsilon) + \varepsilon \mathbf{d}^{n1}(\lambda^\varepsilon) + ... \tag{15}$$

From the definition of $\mathbf{R}^\varepsilon(\tilde{n})$, the position of the nodes, one obtains the following asymptotic expansion of the length of the beams (Mourad (2003))

$$l^{\varepsilon b} = \varepsilon l^{b0} + \varepsilon^2 l^{b1} + ... \tag{16}$$

We shall retain only the dominant term. The superscript '0' indicates that we consider the initial value before any deformation, in coherence with the small deformation framework. The superscript 'ε' indicates that we make the asymptotic expansion of the quantity considered. We consider that for the unit direction vector's of the beams, $\mathbf{e}^{\varepsilon b} = \mathbf{e}^{b0}$ is independent of ε, this means that these vectors are related to the assumptions of small perturbations.

The asymptotic expansion of virtual velocity $\mathbf{v}^\varepsilon$, is written by Taylor series expansion

$$\mathbf{v}^\varepsilon\left(O\left(\tilde{b}\right)\right) - \mathbf{v}^\varepsilon\left(E\left(\tilde{b}\right)\right) = \mathbf{v}(\lambda^\varepsilon) - \mathbf{v}(\lambda^\varepsilon + \varepsilon \delta^{ib}) = -\varepsilon \frac{\partial \mathbf{v}(\lambda^\varepsilon)}{\partial \lambda^i} \delta^{ib} + ... \tag{17}$$

Regarding the asymptotic expansion of the forces, we will use the mechanics of beams, considering an Euler-Bernoulli model. In the present 2D case, the unit vector $\mathbf{e_3}$ in Cartesian coordinate system is normal to the planar lattice. A vector $\mathbf{e}^{b\perp}$ is introduced, as the unit transversal vector for beam b, viz

$$\mathbf{e}^{b\perp} = \mathbf{e_3} \wedge \mathbf{e^b} \tag{18}$$

The force exerted on beam b

$$\mathbf{T}^{\varepsilon\mathbf{b}} = N^{\varepsilon b}\mathbf{e^b} + T_t^{\varepsilon b}\mathbf{e^{b\perp}} \tag{19}$$

decomposes into the normal force

$$N^{\varepsilon b}\mathbf{e^b} = \frac{E_s S^{\varepsilon b}}{l^{\varepsilon b}} \left((\mathbf{d}^\varepsilon (E (b)) - \mathbf{d}^\varepsilon (O (b))) . \mathbf{e^b} \right) . \mathbf{e^b} \tag{20}$$

and a transverse force

$$T_t^{\varepsilon b}\mathbf{e^{b\perp}} = \frac{12E_s I_z^\varepsilon}{(l^{\varepsilon b})^3} \left((\mathbf{d}^\varepsilon (E (b)) - \mathbf{d}^\varepsilon (O (b))) . \mathbf{e^{b\perp}} \right) . \mathbf{e^{b\perp}} \tag{21}$$

E_s represents the Young's modulus of the beam material, $S^{\varepsilon b}$ is the beam section (the beam section is supposed rectangular, with a unit thickness). Another choice could have to be done without harming the demonstration. In the case of a rectangular section, the section of the beam is $S^{\varepsilon b} = t^{\varepsilon b}$. I_z is the quadratic moment of the beam.

The order in ε of the development of the section t^ε is obtained from the density ρ^* of the lattice, which is constant, independent of ε, scaled as

$$\rho^* \propto \frac{t^{\varepsilon b}}{l^{\varepsilon b}} \tag{22}$$

From this relation, it follows

$$t^{\varepsilon b} \propto l^{\varepsilon b} \tag{23}$$

If one develops this relation as the equation (16), we obtain

$$t^{\varepsilon b} = \varepsilon t^{b0} + \varepsilon^2 t^{b1} + .. \tag{24}$$

Retaining only the dominant term, we get the quadratic moment for a beam of rectangular section and unit thickness

$$I_z^\varepsilon = \frac{\left(\varepsilon t^{b0} \right)^3}{12} \tag{25}$$

Due to the presently adopted method which relies on beam mechanics, the transverse force differs from the one given in (Mourad (2003); Caillerie et al. (2006); Tollenaere and Caillerie (1998); Raoult et al. (2008)); the interest of the present method is explained in more details in the subsequent paragraph 2.1.4.

It remains to express the displacement difference between the extremity nodes of a beam; a Taylor series development leads to

$$\mathbf{d}^\varepsilon (O (b)) = \mathbf{d}^0 (\lambda^\varepsilon) + \varepsilon \mathbf{d}^{O_R(b)1} (\lambda^\varepsilon) + ... \tag{26}$$

$$\mathbf{d}^\varepsilon (E (b)) = \mathbf{d}^0 \left(\lambda^\varepsilon + \varepsilon\delta^{ib} \right) + \varepsilon \mathbf{d}^{E_R(b)1} \left(\lambda^\varepsilon + \varepsilon\delta^{ib} \right) + ... =$$
$$\mathbf{d}^0 (\lambda^\varepsilon) + \varepsilon\frac{\partial \mathbf{d}^0(\lambda^\varepsilon)}{\partial \lambda^i}\delta^{ib} + \varepsilon \mathbf{d}^{E_R(b)1} (\lambda^\varepsilon) + \varepsilon^2 \frac{\partial \mathbf{d}^{E_R(b)1}(\lambda^\varepsilon)}{\partial \lambda^i}\delta^{ib} + ... =$$
$$\mathbf{d}^0 (\lambda^\varepsilon) + \varepsilon \left(\frac{\partial \mathbf{d}^0(\lambda^\varepsilon)}{\partial \lambda^i}\delta^{ib} + \mathbf{d}^{E_R(b)1} (\lambda^\varepsilon) \right) + ... \tag{27}$$

$$\mathbf{d}^\varepsilon\left(E\left(b\right)\right) - \mathbf{d}^\varepsilon\left(O\left(b\right)\right) = \varepsilon\left(\mathbf{d}^{E_R(b)1}\left(\lambda^\varepsilon\right) - \mathbf{d}^{O_R(b)1}\left(\lambda^\varepsilon\right) + \frac{\partial \mathbf{d}(\lambda^\varepsilon)}{\partial \lambda^i}\delta^{ib}\right) + ... \tag{28}$$

with$\mathbf{d}^{E_R(b)1}\left(\lambda^\varepsilon\right)$ and $\mathbf{d}^{O_R(b)1}\left(\lambda^\varepsilon\right)$ the unknown displacements of the reference nodes within the unit cell. We show in section (2.1.3) how to solve these unknowns. In order to simplify the following developments we define

$$d\mathbf{D}^\varepsilon{}_{EO} = \mathbf{d}^\varepsilon\left(E\left(b\right)\right) - \mathbf{d}^\varepsilon\left(O\left(b\right)\right) = \varepsilon\left(\mathbf{d}^{E_R(b)1}\left(\lambda^\varepsilon\right) - \mathbf{d}^{O_R(b)1}\left(\lambda^\varepsilon\right) + \frac{\partial \mathbf{d}(\lambda^\varepsilon)}{\partial \lambda^i}\delta^{ib}\right) + ... \tag{29}$$

Inserting the equations (24), (25), (28), (16) in the equations defining the forces(20) and (21), one obtains

$$N^{\varepsilon b}\mathbf{e^b} = \frac{E_s t^b}{l^b}(d\mathbf{D}^\varepsilon{}_{EO}.\mathbf{e^b}\,\delta^{ib}).\mathbf{e^b} \tag{30}$$

$$T_t^{\varepsilon b}\mathbf{e^{b\perp}} = \frac{E_s\left(t^b\right)^3}{\left(l^b\right)^3}\left(d\mathbf{D}^\varepsilon{}_{EO}.\mathbf{e^{b\perp}}\,\delta^{ib}\right).\mathbf{e^{b\perp}} \tag{31}$$

If we further insert the last two equations in equation (19), we get

$$\mathbf{T}^{\varepsilon \mathbf{b}} = \frac{E_s t^b}{l^b}(d\mathbf{D}^\varepsilon{}_{EO}.\mathbf{e^b}\,\delta^{ib})\mathbf{e^b} + \frac{E_s\left(t^b\right)^3}{\left(l^b\right)^3}\left(d\mathbf{D}^\varepsilon{}_{EO}.\mathbf{e^{b\perp}}\,\delta^{ib}\right).\mathbf{e^{b\perp}} \tag{32}$$

Finally, if we substitute equations (32) and (17) in(13), the following discrete weak form of equilibrium is obtained

$$\sum_{v^i\in\mathbb{Z}^3}\sum_{b\in\mathcal{B}_R}\left(\frac{E_s t^b}{l^b}(d\mathbf{D}^\varepsilon{}_{EO}.\mathbf{e^b}\,\delta^{ib})\mathbf{e^b} + \frac{E_s\left(t^b\right)^3}{\left(l^b\right)^3}\left(d\mathbf{D}^\varepsilon{}_{EO}.\mathbf{e^{b\perp}}\,\delta^{ib}\right).\mathbf{e^{b\perp}}\right)\cdot\left[\varepsilon\frac{\partial \mathbf{v}(\lambda^\varepsilon)}{\partial \lambda^i}\delta^{ib}\right] \quad = \quad \mathbf{0} \quad (33)$$

We can write this equation in the 2D case in the form

$$\sum_{v^i\in\mathbb{Z}^3}\varepsilon^2\sum_{i\in\{1,2\}}\mathbf{S^i}\cdot\left[\frac{\partial \mathbf{v}(\lambda^\varepsilon)}{\partial \lambda^i}\right] = \mathbf{0} \tag{34}$$

In this equation the vector $\mathbf{S^i}$ can be defined as

$$\mathbf{S^i} = \sum_{b\in\mathcal{B}_R}\left(\frac{E_s t^b}{l^b}(d\mathbf{D}^\varepsilon{}_{EO}.\mathbf{e^b}\,\delta^{ib})\mathbf{e^b} + \frac{E_s\left(t^b\right)^3}{\left(l^b\right)^3}\left(d\mathbf{D}^\varepsilon{}_{EO}.\mathbf{e^{b\perp}}\,\delta^{ib}\right).\mathbf{e^{b\perp}}\right)\delta^{ib} \tag{35}$$

Hence, $\mathbf{S^i}$ can be expressed in the condensed form

$$\mathbf{S^i} = \sum_{b\in\mathcal{B}_R}\left(\mathbf{N}^b + \mathbf{T}_t^b\right)\delta^{ib} \tag{36}$$

We next use the following result (Mourad (2003)) to transform the discrete into a continuous equilibrium formulation: "for any sufficiently regular function g, the quantity $\varepsilon^2\sum_{v^i\in\mathbb{Z}^3}g(\varepsilon v^i)$ can be interpreted as a Riemann sum of an integral over Ω. It tends to$\int_\Omega g(\lambda)d\lambda$ as ε goes to 0". Thus, using this proposition, the equation (34) can be written

$$\int_\Omega \mathbf{S^i}\cdot\frac{\partial \mathbf{v}(\lambda^\varepsilon)}{\partial \lambda^i}d\lambda \tag{37}$$

From the stress vectors $\mathbf{S^i}$, and using equation (9), one can then formulate the stress tensor σ as

$$\sigma = \frac{1}{g}\mathbf{S^i}\otimes\frac{\partial \mathbf{R}}{\partial \lambda^i} \tag{38}$$

Observe that the macroscopic variables naturally follow from the homogenization technique, and there is no need to define the macroscopic fields as averages of their microscopic counterpart, as in classical homogenization methods.

The automatic treatment of the steps of the discrete homogenization has been implemented in a Maple code; these steps are summarized in the following algorithm 1. In the examples to be treated next, only lattices with fixed unit vectors in the curvilinear system have been considered. To avoid confusion in notations, the vectors of the curvilinear coordinates are denoted $\mathbf{Y_i} = \mathbf{e_i^\lambda}$, and the Cartesian vectors $(\mathbf{i}, \mathbf{j}, \mathbf{k}) = (\mathbf{e}_1, \mathbf{e}_2, \mathbf{e}_3)$. The lattice topology can be modified by simply rewriting a text file describing its geometry and connectivity.

Algorithm 1 Algorithm for the automatized discrete homogenization

1. Initialization of the tables of initial data. Definition of the function $\mathbf{R}$ such that : $\mathbf{x} = \mathbf{R}(\lambda^1, \lambda^2, \lambda^3)$

2. Transformation of the expression $\left(\dfrac{\partial \mathbf{d}}{\partial \lambda_i}\right)_{(\mathbf{e_1^\lambda}, \mathbf{e_2^\lambda})} \mapsto \left(\dfrac{\partial \mathbf{d}}{\partial \lambda_i}\right)_{(\mathbf{e}_1, \mathbf{e}_2)}$. (to avoid confusion in examples and the Maple code, the vectors of curvilinear system are denoted $\mathbf{Y_i} = \mathbf{e_i^\lambda}$, the vectors of Cartesian system are denoted $(\mathbf{i}, \mathbf{j}, \mathbf{k}) = (\mathbf{e}_1, \mathbf{e}_2, \mathbf{e}_3)$).

3. Decomposition of the resultant $\mathbf{T^b} = \mathbf{N}^b + \mathbf{T}_t^b$, sum of the normal and transverse forces $\mathbf{N}^b, \mathbf{T}_t^b$, versus the displacement unknowns $\mathbf{d}^{E_R(b)1}(\lambda^\varepsilon)$, $\mathbf{d}^{O_R(b)1}(\lambda^\varepsilon)$ and the first order Taylor series expansions of $\mathbf{d}^0$.

4. Solution of the self-equilibrium equations (equilibrium at each node) $\sum\limits_{b\in\mathcal{B}_R} \mathbf{T^b} \cdot [\mathbf{v}(O(b)) - \mathbf{v}(E(b))] = \mathbf{0}$

5. Expression of the stress vector $\mathbf{S^i} = \sum\limits_{b\in\mathcal{B}_R} \left(\mathbf{N}^b + \mathbf{T}_t^b\right)\delta^{ib}$

6. Calculation of the stress tensor $\sigma = \dfrac{1}{g}\mathbf{S^i} \otimes \dfrac{\partial \mathbf{R}}{\partial \lambda^i}$

7. Calculation of effective properties

2.1.3 Self-equilibrium equations and evaluation of the displacement unknowns in the case of internal nodes

The truss equilibrium implies the unit cell (or reference cell) equilibrium. The equation (12) can be rewritten in the form

$$\sum_{b\in\mathcal{B}_R} \mathbf{T^b} \cdot [\mathbf{v}(O(b)) - \mathbf{v}(E(b))] = \mathbf{0} \tag{39}$$

with $\mathcal{B}_R$ the list of nodes for the reference cell. Equation (39) can be expanded into as many independent equations as internal nodes, since it applies for any nodal velocity $\mathbf{v}(.)$; the resulting system of equations allows to solve for the unknown displacements $\mathbf{d}^{E_R(b)1}(\lambda^\varepsilon)$ and $\mathbf{d}^{O_R(b)1}(\lambda^\varepsilon)$ of the reference nodes within the unit cell.

2.1.4 Interest of the adopted definition of the transverse force $\mathbf{T}_t^b$

The method developed in Mourad (2003) and Caillerie et al. (2006) uses the moment equilibrium equation to replace the expression of the transverse forces $\mathbf{T}_t^b$ in the equation (13) by the couple M generated by the angular variation between two consecutive beams. This modeling approach is customary in the field of applications considered by the authors, namely molecular dynamics or interatomic physics, with an application to carbon nanotube's microstructure. The authors adopt the mechanics of interacting bars, whereas we choose beam mechanics for the description of the lattice behavior. In our treatment, the expression of the couple stresses and thereby of the transverse forces is linked to the difference of displacements between the extremity nodes of a given beam. Figure (3) shows the difference between both methods (considering the linearized method adopted in Caillerie et al. (2006)). In present approach the couple is a fonction of the displacement difference between the end nodes of a beam. Caillerie and al. use the angular variation between two beams in Caillerie et al. (2006).

Moreover, in order to be able to use the rotational equilibrium equations, the previous authors identify the rotation
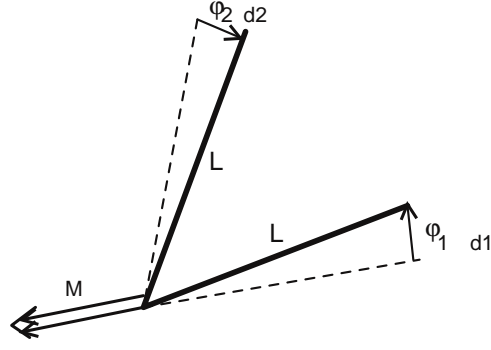
(a) Couple due to the angular variation between two bars (Caillerie et al. (2006))
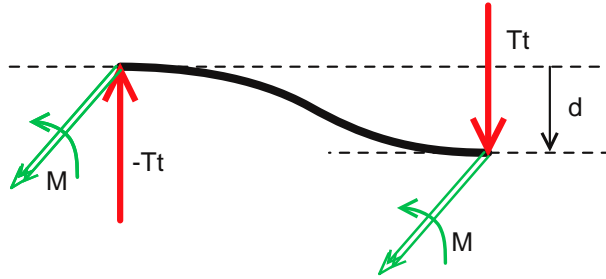
(b) Couple generated by the displacement difference between the end nodes of the same beam (present work)

Figure 3: Differences between the couples in the present method and in Caillerie et al. (2006)

of the beam to a rigid body motion, implying the assumption of beams without internal transverse force. We adopt, to the contrary, the beam theory, with the couple considered as an internal moment.

The assumption adopted in the present treatment of couples simplifies the problem formulation, since one does not need the moment equilibrium to solve the problem, assuming no node rotations. This method offers additionally interesting perspectives: when considering node rotations, the couple equilibrium equations shall furnish additional equations allowing the extension of the present model to the construction of micro-polar continua by homogenization, which seems impossible with the method developed by Caillerie et al. (2006).

2.2 Test on a 2D "hexagonal" or "honeycomb" lattice under compression

The geometry of the 2D honeycomb lattice is shown in the previous Figure 1, assuming for a regular hexagonal lattice the geometrical constraints $h = l$ and $\theta = 30°$. The effective Young's modulus, the Poisson's coefficient and relative density are given versus the microbeam length l, width t and the microbeam modulus E_s

$$E^* = \frac{4 E_s t^3 \sqrt{3}}{3l(l^2 + 3t^2)} \tag{40}$$

$$\nu_{12}^* = \frac{l^2 - t^2}{l^2 + 3\,t^2} \tag{41}$$

$$\rho^* = \frac{2}{3} \frac{t\sqrt{3}}{l} \tag{42}$$

One can observe that in the case of slender beams (beams with a large length to width ratio, viz $l \gg t$), the previous expression of the effective traction modulus (40) becomes $E^* = \dfrac{4 E_s t^3 \sqrt{3}}{3l^3}$, which is identical to the
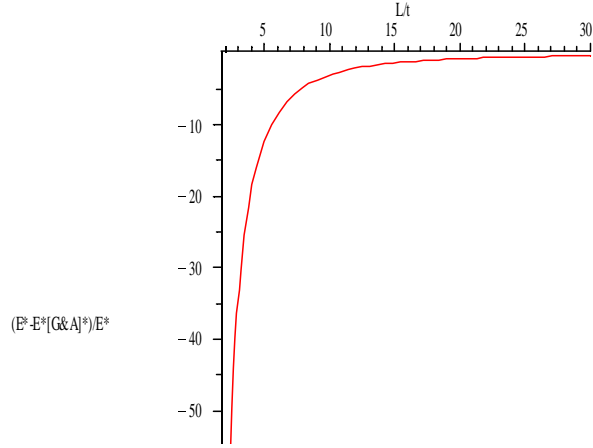
Figure 4: Evolution of the relative value (in percent) between the effective modulus for a hexagonal lattice in (Gibson (2005); Gibson and Ashby (1997)) and the homogenized modulus, vs. the ratio L/t.

formula obtained by various authors (Gibson (2005); Gibson and Ashby (1997)). One can further explore a wider range of beam length to width ratio; we focus on ratios that are comparable or less than unity. The Figure 4 shows a discrepancy of the effective properties with the Gibbson and Ashby results: for a ratio about 5, the relative error is about 10%, and it further increases with decreasing values of l/t. Note, however, that in this case the initial assumption of slender beams looses its validity.

A numerical simulation has been performed, in order to test whether the homogenized expression of the modulus, incorporating compression effects, is more accurate than the Gibson and Ashby formula Gibson (2005); Gibson and Ashby (1997). The mechanical properties of aluminum have been adopted for the microbeams of the lattice, viz

$$E_s = 72000 \, N/mm^2$$

$$\nu = 0.33$$

To minimize edge effects inherent to such simulations on finite domains, we use a lattice with 16x16 cells (judged as including a sufficiently large number of cells). The edge condition's consists of blocked rotations, the node at the bottom left is fixed, with all bottom nodes having a fixed vertical displacement (Figure 5). Both a Bernoulli type element (no shear, Abaqus beam element B23), or a Timoshenko type element incorporating shear (Abaqus element B22), have been considered. This last element is more adequate in the case of beams with a relatively small length to width ratio. The considered sample being simulated represents an area of 1mm^2, with a relative density $\rho^* = 0.15$, corresponding to beam elements with length 0.0385 mm and width 0.005 mm, endowed with a rectangular section. FE simulations with a higher density $\rho^* = 0.24$ will also be performed (the width is 0.008 mm), corresponding to a length over width ratio of 5. The FE results of virtual compression tests are exploited in terms of the equivalent modulus (normalized to the material modulus) and Poisson's ratio; considering the external nodes (average of two nodal values on each edge), the following definitions of the numerical homogenized properties are adopted

$$\frac{E^*}{E_s}_{(FE)} = \frac{\sigma_{22}}{\varepsilon_{top} E_s} \tag{43}$$

$$\nu^*_{12(FE)} = \frac{\varepsilon_{lateral}}{\varepsilon_{top}} \tag{44}$$

with self explanatory notations. As the linear dimension of the cube is 1 mm, and since the modulus of the microbeam E_s is expressed in units of N/mm, the longitudinal and lateral sample deformations follow from the edge displacements as

$$\varepsilon_{top} = U2_{topnode} \tag{45}$$
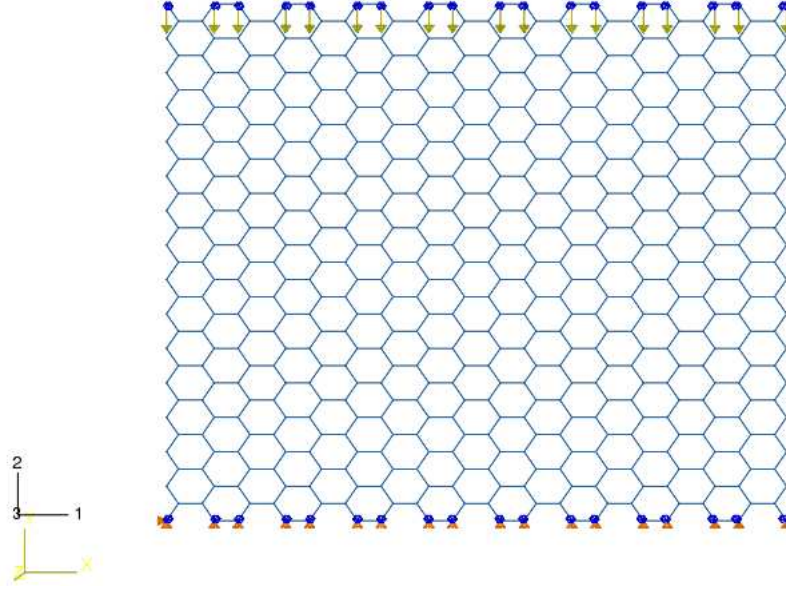
Figure 5: Geometry of the hexagonal truss and its boundary conditions

Beam width and element type	Homogenized properties (this work)	FE results	G&A results
Bernouilli, t=0.005mm	$E^* = 347$MPa, $\nu_{12}^* = 0.94$	$E^* = 355$MPa, $\nu_{12}^* = 0.97$	$E^* = 364$MPa, $\nu_{12}^* = 1$
Bernouilli, t=0.008mm	$E^* = 1321$MPa, $\nu_{12}^* = 0.85$	$E^* = 1368$MPa, $\nu_{12}^* = 0.88$	$E^* = 1492$MPa, $\nu_{12}^* = 1$
Timoshenko, t=0.005mm	$E^* = 347$MPa, $\nu_{12}^* = 0.94$	$E^* = 338$MPa, $\nu_{12}^* = 0.97$	$E^* = 364$MPa, $\nu_{12}^* = 1$
Timoshenko, t=0.008mm	$E^* = 1321$MPa, $\nu_{12}^* = 0.85$	$E^* = 1222$MPa, $\nu_{12}^* = 0.90$	$E^* = 1492$MPa, $\nu_{12}^* = 1$

Table 1: Results obtained for the mechanical properties of a hexagonal lattice

$$\varepsilon_{lateral} = U1_{rightnode} - U1_{leftnode} \tag{46}$$

$U1$, $U2$ denote the horizontal and vertical displacements, respectively.

The FE results (Figure 6) as apparent from the detailed view of the mesh distortion (see the insert of Figure 6b) show that the initial assumption related to the deformation mode of the microbeams in the truss is validated: there is obviously no rotation of the edge nodes in this compression loading mode.

2.1.5 Comparison of effective homogenized properties with FE results and literature values

The homogenized elastic properties are compared with FE results and to the Gibson and Ashby Gibson and Ashby (1997) results in the Table 1.

This Table 1 highlights the following points:

- Homogenized properties are closer to the FE values, and a discrepancy with the Gibson and Ashby results is observed for both densities.

- The evolution pictured in Figure 4 reflects the discrepancy between the analytical results of Gibson and Ashby and FE results.

- A supplementary effect due to the micro-beam shear exists, which cannot be neglected when the length to a width ratio is less than 5 (for a beam with width t=0.008). This effect is not taken into account by the present code, based on a Bernouilli beam element.

(a) FE simulation of the hexagonal lattice under compression

(b) Zoom on the microbeam deformation
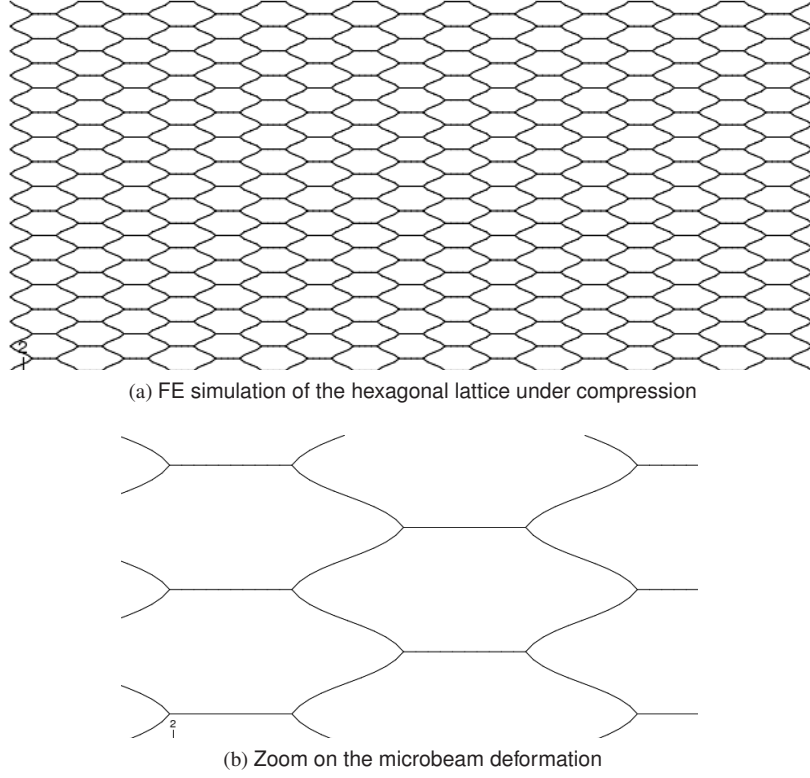
Figure 6: Hexagonal lattice under compression

2.2 A mixed flexional extensional lattice: the 2D "OctogonMixed" lattice

Since a shear loading is prone to induce flexion (whereas no flexion will generally accompany compression tests), we have conceived and generated a 2D 'OctogonMixed' lattice. This lattice first illustrates the power of the asymptotic homogenization technique, in comparison to other approaches, like the energetical method, which may not work for complex lattice topologies. In the discrete homogenization, we will not use assumptions of average quantities on a cell or assumptions related to the mathematical form of displacement fields in the unit cell. We rather use the mechanical equilibrium at the nodes; this improves the consistency of results from a mechanical point of view. Perhaps more importantly, this lattice is novel in itself, since it can represent a mixed continuous flexional / extensional behavior, when the topology is varied according to a process being described in the sequel.

2.2.1 Homogenized properties

A new lattice having the ability to account in a flexible manner to both extensional and flexional behavior has been conceived (Figure 7), coined the "OctogonMixed" lattice.

The relative length of diagonal versus axial beams has been parametrized by the scalar r

$$L_a = (1 - r) \cdot L \tag{47}$$

$$L_d = r \cdot L/\sqrt{2} \tag{48}$$

with L_a length of vertical and horizontal beams, and L_d length of diagonal beams.

Thereby, one can span a wide spectrum of behaviors, from purely extensional ones with $r = 0$ corresponding e.g. to the tetragonal lattice, to a purely flexional behavior when $r = 1$, corresponding to a 'diamond' type lattice; intermediate values of the parameter r describe a lattice with a mixed flexional and extensional behavior. The width t_a of the axial beams has here been taken as $t_a = t_d/10$. The width of diagonal beams is denoted $t = t_d$. As
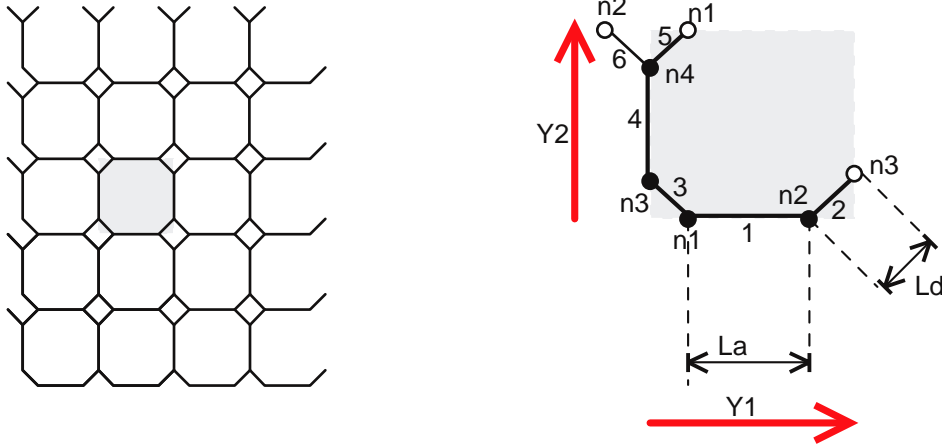
Figure 7: The"OctogonMixed" lattice. (The nodes with a solid circle belong to the reference cell. The nodes with a hollow circle belong to adjacent cells)

regard to the boundary conditions, the edge nodes are clamped and no rotational d.o.f. of the nodes are considered. The homogenized properties are obtained as follows

$$E_1^* = 2 \, \frac{kld \; kla \; kpd}{kla \; kld + 2 \; kld \; kpd + kla \; kpd} \tag{49}$$

$$\nu_{12}^* = \frac{kla \; (kld - kpd)}{kla \; kld + 2 \; kld \; kpd + kla \; kpd} \tag{50}$$

$$\rho^* = \frac{1/5 \; (1-r) \, Lt + 2 \, rL\sqrt{2}t}{L^2} \tag{51}$$

The same properties result for the second axis, due to the isotropy of the equivalent continuum material. The variables $kla = kld = E_s t_i / L_i$ in the expressions above are the axial moduli of the microbeams, with t_i, L_i their width and length, respectively, and $kpa = kpd = 12 E_s I_z / L_i^3$ the flexion moduli.

2.2.2 Comparison with FE results

The geometrical and mechanical (aluminum) characteristics are those of the previously described honeycomb lattice.

In order to avoid the critical buckling load (given by $F_c = 4\pi E_s I / L^2$ in a bi-clamped configuration), a distributed compressive load of 1N / mm has been considered. The edge (boundary) conditions are blocked rotations on the external edges, the left bottom node fixed, and the other bottom nodes have a fixed vertical displacement. The Bernouilli type element is selected, so as to match the FE mesh with the discrete topology of the lattice, adopting 3 elements per beam. The sample is a 2D cube with dimension 1x1 mm^2, with a constant density $\rho^* = 0.15$. In order to avoid edge effects, one considers a 16x16 cell lattice, with edge beams having a width divided by a factor two, compatible with the applied loading. The equivalent elastic properties are defined similarly to the honeycomb lattice, according to the following formulas (σ is the compression load)

$$\frac{E^*}{E_s}_{(FE)} = \frac{\sigma}{\varepsilon_{top} E_s} \tag{52}$$

$$\nu_{12(FE)}^* = \frac{\varepsilon_{lateral}}{\varepsilon_{top}} \tag{53}$$

98
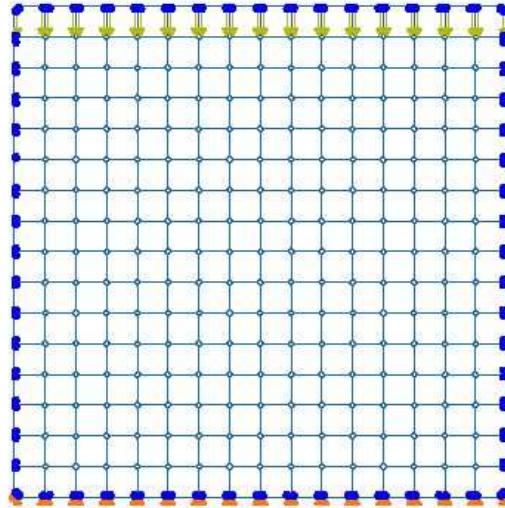
(a) loads
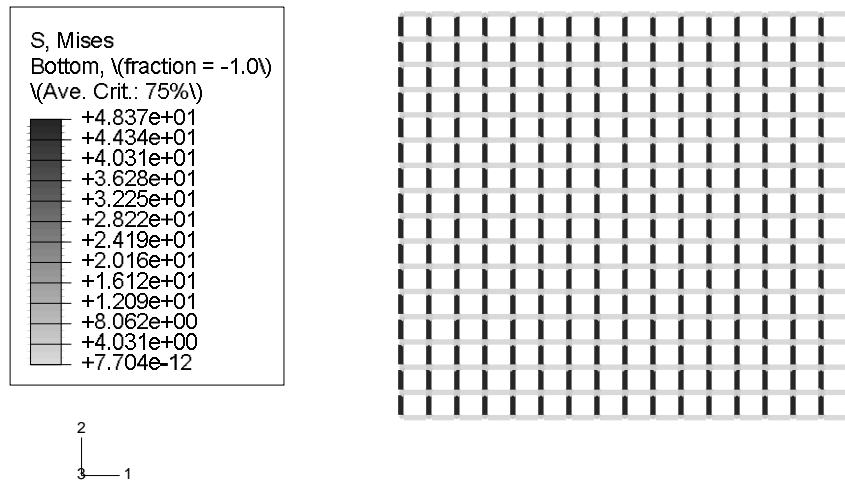
(b) stress distribution

Figure 8: OctogonMixed lattice. Von Mises stress distribution. $r = 0.2$

As the cube has a linear dimension 1 mm, and the modulus of the microbeam E_s is expressed in N/mm, the longitudinal and transversely strains are defined as before. Observe that the homogenized modulus in the compression direction (y) is presently obtained, viz $E_2 = E^*$. Simulation results for this lattice are shown in Figure 8, 9 and 10.

The distribution of the stresses reflects the progressive change of the deformation mode of this truss from dominant extension (for r=0.2: the stresses are distributed mostly in the horizontal and vertical beams) to dominant flexion (for $r = 0.8$). For the intermediate situation ($r = 0.5$), the stresses are distributed in a relatively uniform manner in both axial and transverse beams, witnessing this truss has no more dominant deformation mode. Homogenized and FE simulated moduli are compared in the Table 2.

The Table 2 shows identical results, which validates the calculation steps of the discrete homogenization for this lattice. Since the truss is parametrized by the scalar r, allowing a transition from a lattice working under pure compression to pure flexion, it is interesting to record the evolution of the effective modulus (normalized by the microbeam modulus) versus the parameter r. Considering a constant density, the Figure 11a shows that flexional trusses are considerably less rigid compared to trusses working in traction/compression. This behavior may have
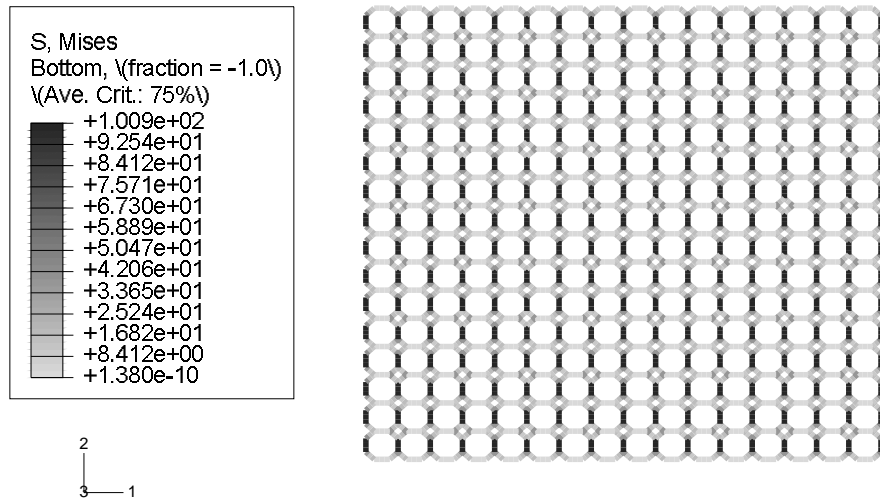
Figure 9: OctogonMixed lattice. $r = 0.5$. Von Mises stress distribution
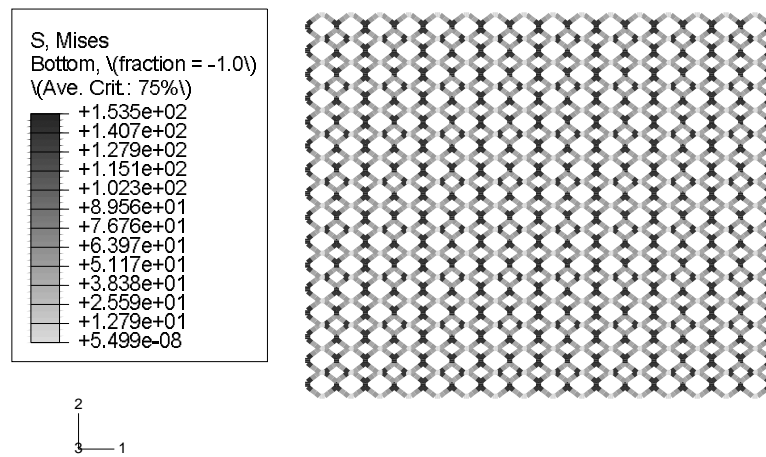
(a) stress distribution
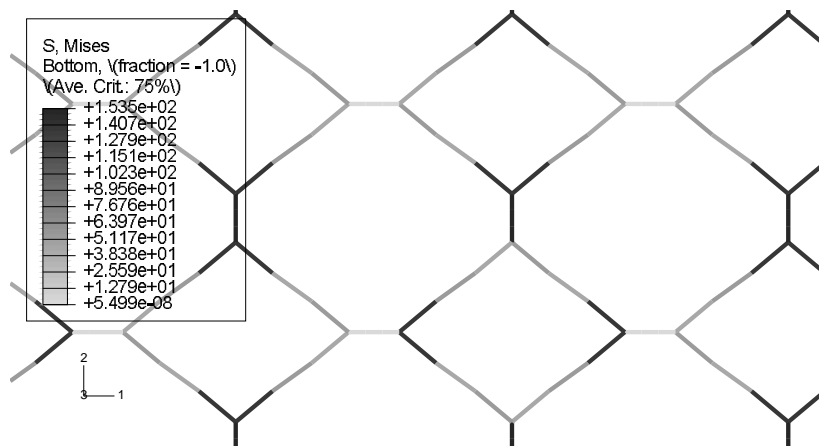
(b) Von Mises stress distribution. zoom from previous Figure

Figure 10: OctogonMixed lattice. $r = 0.8$. Von Mises stress distribution

Relative length of diagonal versus axial beams	Effective properties from homogenization	FE results
$r = 0.2$	$E^*/E_s = 0.0255\,\nu_{12} = -0.00464$	$E^*/E_s = 0.0255\,\nu_{12}^* = -0.00464$
$r = 0.5$	$E^*/E_s = 0.0133\,\nu_{12} = 0.279$	$E^*/E_s = 0.0133\,\nu_{12}^* = 0.279$
$r = 0.8$	$E^*/E_s = 0.00276\,\nu_{12} = 0.891$	$E^*/E_s = 0.00276\,\nu_{12}^* = 0.891$
$r = 1$	$E^*/E_s = 0.000839\,\nu_{12} = 0.989$	$E^*/E_s = 0.000839\,\nu_{12}^* = 0.989$

Table 2: Results for OctogonMixed lattice
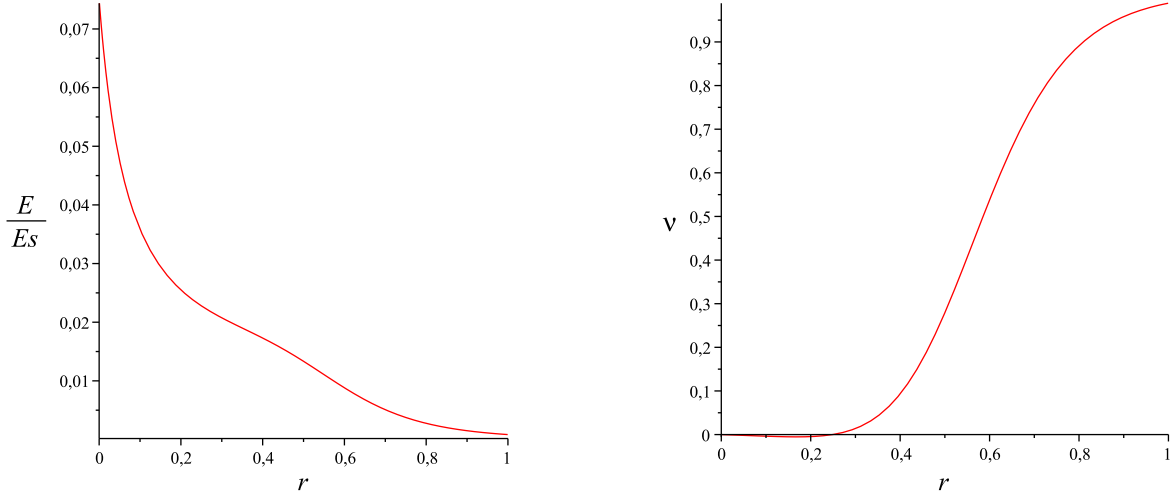
(a) Evolution of the Young's modulus E^*/E_s, of the OctogonMixed lattice, when moving from square to diamond lattice

(b) Evolution of the Poisson coefficient of the OctogonMixed lattice, when moving from square to diamond lattice, at constant equivalent density $\rho^* = 0.15$

Figure 11: Evolution of homogenized elastic properties versus parameter r

important consequences as to the mechanical response of a lattice under traction/compression presenting damaged beams.

It is interesting to note from the Figure 11b that the lattice may exhibit a slightly negative value of the Poisson coefficient, due to the behavior of the diagonal beams of the diamond structure.

It is worthwhile recording the evolution of the coefficient n, according to Figure 12: numerous authors in the literature propose in order to simplify the lattice calculations a generic formula of the type

$$E^* = C\,E_s(\rho^*)^n \tag{54}$$

with C constant.

In Gibson (2005); Gibson and Ashby (1997), the values $n = 2$ (the effective modulus scales as the square of the lattice density) and $C\,1$ are adopted for the 2D hexagonal and the 3D tetrakaidecahedron lattice.

Although these values are convenient for specific lattices, it becomes clear that they do not reflect the true complex behavior of more general lattices, as the present one: the Figure 12 shows that it is not possible to assign a fixed value for the exponent n. This is further confirmed by Roberts and Garboczi (2002), who state that experiments lead to values of the exponent in the range $1 < n < 4$, with a dependency of the equivalent modulus upon density being rather obscure.

As for the hexagonal truss, inconsistent effective properties are obtained under a shear test, as reflected by the compliance matrix
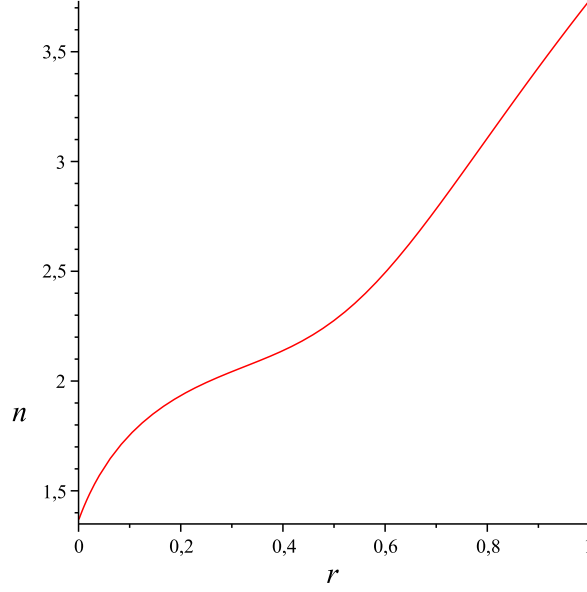
Figure 12: Evolution of the exponent n, as $\dfrac{E}{E_s} = (\rho^*)^n$ for the OctogonMixed lattice when moving from square to diamond lattice, at constant relative density $\rho^* = 0.15$

$$S = \begin{bmatrix} S_{11} & S_{12} & 0 & 0 \\ S_{21} & S_{22} & 0 & 0 \\ 0 & 0 & S_{33} & S_{34} \\ 0 & 0 & S_{43} & S_{44} \end{bmatrix} \tag{55}$$

with $S_{11} = S_{22} = \frac{kla.kld+2.kpd.kld+kla.kpd}{2(kld.kla.kpd)}$, $S_{21} = S_{12} = S_{34} = S_{43} = -\frac{kld-kpd}{2(kpd.kld)}$ and $S_{33} = S_{44} = \frac{kpa.kld+kpa.kpd+2.kpd.kld}{2(kpa.kld.kpd)}$

(We recall that the variables $kla = kld = E_s t_i/L_i$ are the axial moduli, and $kpa = kpd = 12E_s I_z/L_i^3$ the flexion moduli)

Due to the mechanical equilibrium of the cell, the coefficient S_{33} and S_{43} should be equal, as well as coefficients S_{34} and S_{44}. Hence, inconsistent expressions of the shear modulus G will result, due to the too restrictive boundary conditions, that prevent edge rotations. This points towards the need to enhance the kinematics and the statics of both the lattices and their equivalent continuum to account for rotational d.o.f., especially when shear loadings are involved.

2.3 A proposal for classification of lattices with respect to rotations

Lattices may be classified with respect to the consideration of rotational d.o.f., according to the nature of the applied loading. The equivalent continuum model must reflect the mechanical behavior - and especially the deformation modes - of the underlying microscopic discrete material: this coherency has to be reflected in the choice of the kinematic descriptors at the macro scale, so that the macroscopic kinematics matches the microscopic one. In particular, and as indicated in the previous examples, the consideration of rotational microscopic d.o.f. points towards the consideration of a micropolar continuum model at the macroscopic level.

In order to substantiate the argumentation, let write the fundamental energy principle for beams in the absence of torsion and forces, and with moments only applied to the boundaries (Pedro et al. (2004))

$$\underbrace{\frac{1}{2}\sum(F_i\delta_i + C_i\alpha_i)}_{\text{Clapeyron's formula}} = \frac{1}{2}\int\left(\frac{N^2}{ES} + \frac{M_f^2}{EI}\right)ds \tag{56}$$

(a) PU foam Gibson (2005)   (b) nickel foam (Badiche et al. (2000))
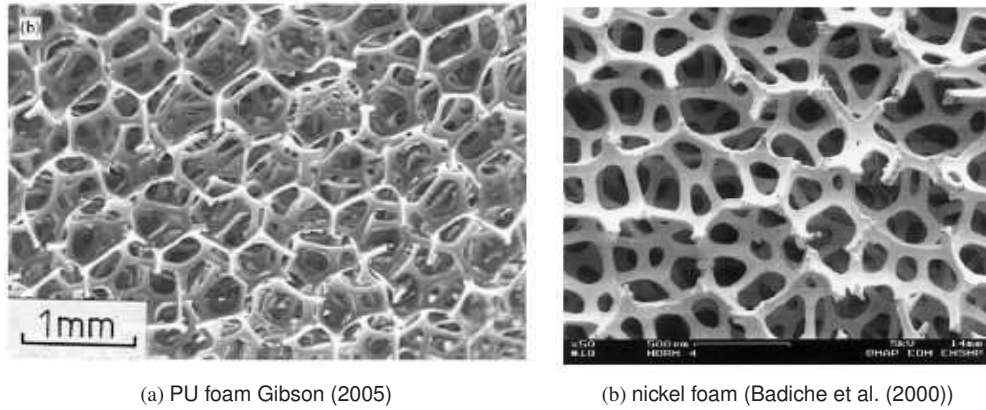
Figure 13: Examples of various foams with an architecture close to the tetrakaidecahedral truss
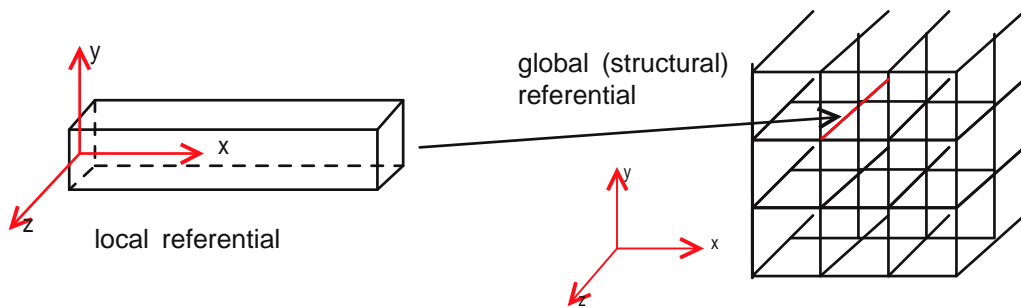
Figure 14: Transition from the local beam referential to the structural referential

This equality relates (twice) the internal work of the force and moment of flexion, viz the variables N, M_f respectively, to the external work of the applied force and couple, the variables F_i, C_i respectively (working in the displacement and rotation variables (δ_i, α_i) respectively). Due to the virtual nature of the kinematic variables in the previous equation, it appears that the absence of boundary rotations does not induce a corresponding energetic term involving flexion: hence, one may assume the absence of node rotation when no flexion is applied to the boundaries of the sample. Accordingly, the present argumentation together with the previous examples induces the following classification of lattices

- Isostatic trusses (according to the generalized Maxwell criterion; most of the time the trusses are triangulated) without external moments: a non polar model is sufficient;

- Non isostatic trusses with flexion moments / clamped beams / no edge rotation: a non polar model is sufficient;

- Trusses with flexion moments and edge nodes rotation: a micropolar model is then needed.

3   Extension to 3D: case of the Kelvin foams

The extension of the discrete homogenization to 3D has been exemplified for the tetrakaidecahedral truss, a lattice considered as descriptive for the so called Kelvin foams, which still foster many studies nowadays. The reason of this interest stems from the fact that it models in a relatively faithfull manner the geometry of various foams (polymeric and metallic), such as polyurethane or nickel foams (Figure 13).

From a technical point of view, one specific difficulty in extending the discrete homogenization to 3D is the passage from the local referential of the beam to the global referential of the whole structure (Figure 14).

Let us consider a beam aligned with x in its local referential; the passage to the global referential is obtained by
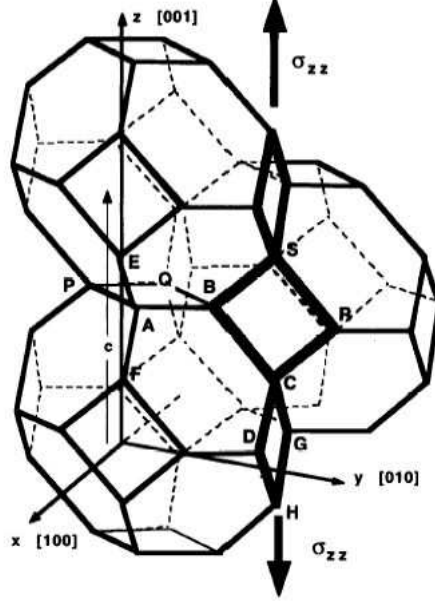
Figure 15: Modified tetrakaidecahedron with planar facets (Zhu et al. (1997))

the combination of a rotation along z, followed by a rotation along x. One has accordingly

$$
R_z = \begin{bmatrix} c_\alpha & -s_\alpha & 0 \\ s_\alpha & c_\alpha & 0 \\ 0 & 0 & 1 \end{bmatrix}
\qquad\qquad
R_x = \begin{bmatrix} 1 & 0 & 0 \\ 0 & c_\beta & -s_\beta \\ 0 & s_\beta & c_\beta \end{bmatrix}^{[1]}
$$

This delivers the transition matrix as

$$
P_{beam\rightarrow structure} = R_x R_z = \begin{bmatrix} c_\alpha & -s_\alpha & 0 \\ c_\beta s_\alpha & c_\beta c_\alpha & -s_\beta \\ s_\beta s_\alpha & s_\beta c_\alpha & c_\beta \end{bmatrix}
\tag{57}
$$

which has to applied to the three axis of the local referential of the beam. Observe that the beam is here endowed with identical quadratic moments Ix and Iz; otherwise, one would need to add a rotation in the transition matrix. The technical complexity of calculating the effective properties from the lattice geometry and mechanical parameters has here been reduced by the implementation of the steps of the asymptotic homogenization in a Maple code specifically devoted to this purpose. This constitutes a novel aspect in the present work, as it allows the calculation of the effective properties of any truss in a 2D or 3D geometry. As pointed out in the introductory section, such a predictive tools remedies the deficiencies of the classical approaches, which are generally not able to perform the necessary calculations in a reliable manner, or rely on special assumptions to overcome those difficulties.

3.1 Effective behavior of the "Tetrakaidecahedral" truss (Kelvin foams)

The tetrakaidecahedron is considered in the form of a 'BCC lattice'; it has originally been proposed by Thomson (Lord Kelvin) in 1887; it is the sole polyhedron filling space so as to minimize the superficial tension; due to that, a large variety of foams are close to this architecture. Moreover, this polyhedron fulfills Plateau conditions; nevertheless, most of the authors use a slightly modified version of this model configuration in order to dispose of planar surfaces and angles of 120° and 90° (Figure 15).

The truss is described as a the repetition of a set of beams submitted to both flexion and extension. [2].

If one adopts a classical non polar equivalent continuum, one may assume that the beams are clamped with respect

---

[1] c_i indicates cos(i) and s_i sin(i)

[2] The torsion is here not considered.
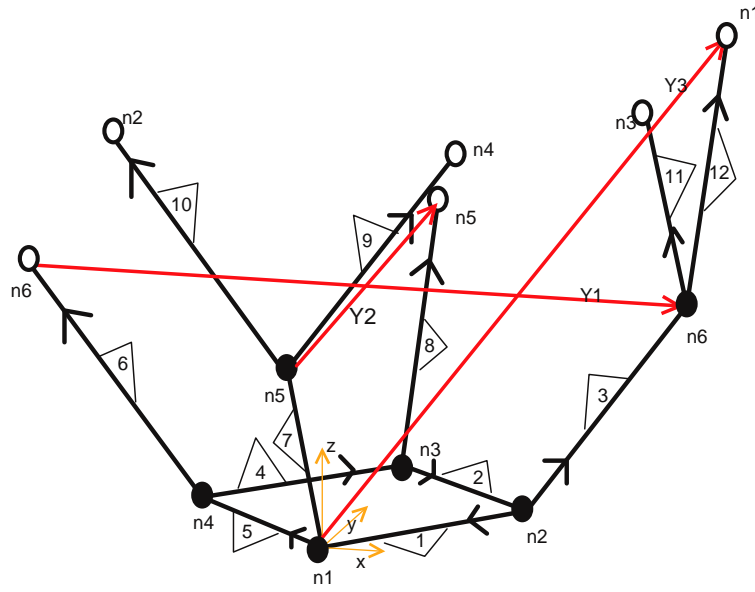
Figure 16: Geometrical representation of the tetrakaidecahedron

to rotation. Moreover, one adopts Bernouilli beam model, hence one has to keep a sufficiently large microbeam length to width ratio, implying in turn low densities. The geometry of the truss is shown in the Figure 16.

The Plateau conditions account for the structure of foam films, amongst other in soap; they have been formulated in the 19[th]century by the belgian physicist Joseph Plateau from observations on soap foams, and proved later on by Jean Taylor from the laws ruling the superficial tension. The following rules follow (Zhu et al. (1997)) :

1. Four Plateau edges intersect under the angle $arccos(-\dfrac{1}{3}) \approx 109, 47°$.

2. The average number of facets per cell is 14.

3. The average number of sides per facet is 5.1.

4. Three arcs meet in the beam section delimiting the edges of a facet (Figure 17) .

These conditions give specific values of the section area and the quadratic moment I

$$A = \sqrt{3}D^2 - \pi D^2/2 \tag{58}$$

$$\frac{I}{A^2} = \frac{20\sqrt{3} - 11\pi}{6(2 * \sqrt{3} - \pi)^2} \tag{59}$$

with D the side dimension. One specific feature of the present geometry is its symmetry, with identical quadratic moments whatever the considered axis, viz $I_z = I_y = I$.

The geometrical (node connectivity, beam length ...) and mechanical description of the lattice, Figure 16 are written in a text file, which feeds the Maple code according to the algorithm 1. We summarize some data of this text file in the Tables 3 and 4

Homogenized properties (traction modulus and Poisson's ratio) are next compared to results from the literature.

105
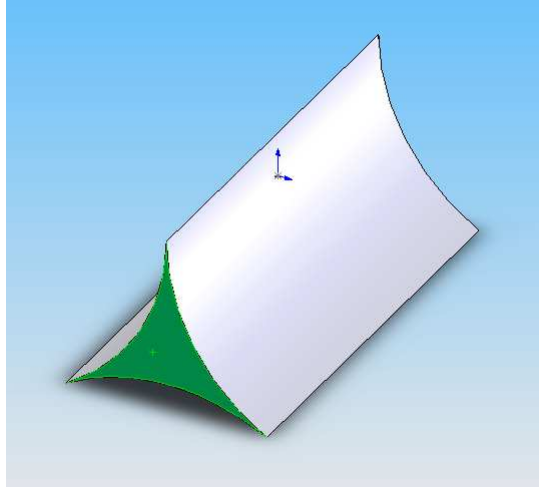
Figure 17: 'Plateau' section in foams

beam	1	2	3	4	5	6	7	8	9	10	11	12
O	2	3	2	3	4	4	1	3	5	5	6	6
E	1	2	6	4	1	6	5	5	4	2	3	1
δ_1	0	0	0	0	0	-1	0	0	0	-1	0	0
δ_2	0	0	0	0	0	0	0	1	-1	-1	-1	0
δ_3	0	0	0	0	0	0	0	0	1	1	1	1

Table 3: Table of node connectivity for tetrakaidecahedron

			Length associated
$\mathbf{Y_1}$		$\begin{bmatrix} -1 \\ 0 \\ 0 \end{bmatrix}$	$2\sqrt{2}L$
$\mathbf{Y_2}$		$\begin{bmatrix} 0 \\ -1 \\ 0 \end{bmatrix}$	$2\sqrt{2}L$
$\mathbf{Y_3}$	$\begin{bmatrix} -1/3\sqrt{3} \\ -1/3\sqrt{3} \\ 1/3\sqrt{3} \end{bmatrix}$		$L\sqrt{6}$

Table 4: Table of generation vector for tetrakaidecahedron

[Gibson and Ashby, 1997Gibson and Ashby (1997)] results: Combining dimensional analysis and experiments, these authors predict that the Young's modulus of PU foams scales versus the equivalent density ρ according to

$$E^* = C_1 E_s (\rho^*)^2; \nu^* = \frac{C_1}{2C_2} - 1$$

with the constants $C_1 \approx 1$ and $C_2 \approx 3/8$. The predicted quadratic dependency upon the equivalent density seems to be confirmed by other studies (both numerical and based on dimensional analysis), with a coefficient C_1 ranging from 0.8 to 1, at least in the weak density regime. (Gibson (2005), Gibson and Ashby (1997)).

Homogenized results (this work): The following set of equivalent properties has been obtained from the asymptotic homogenization technique. The equivalent moduli and Poisson coefficients are equal in both three directions, reflecting an equivalent isotropic material; their expression is given successively by

$$E_1^* = E_2^* = E_3^* = \frac{\sqrt{2}k_b\, k_f}{2(k_b + k_f)}; \nu_{12} = \nu_{23} = \nu_{31} = \frac{k_b - k_f}{2(k_b + k_f)}$$

In this work, with the convention adopted, $E_{010} = E_1^*$, $E_{100} = E_2^*$ and $E_{001} = E_3^*$.

The material parameters $k_b = E_s A/L_i$ in the expressions thereabove are the axial moduli of the microbeams, with A, L_i their section and length, respectively, and $k_f = 12 E_s I / L_i^3$ the flexion moduli; the equivalent density is

$$\rho^* = 1/4 \frac{A \sqrt{6}\sqrt{3}}{L^2}$$

with A being the beam section area.

Zhu et al. (1997) results: the direction with Miller index 100 is presently considered

$$E_{100} = \frac{1.009 E_s (\rho^*)^2}{1 + 1.514\rho^*}; \nu_{12} = \frac{0.5 * (1 - 1.514\rho^*)}{(1 + 1.514\rho^*)}; \rho^* = \frac{3A}{2\sqrt{2}L^2}$$

with A the beam section area.

Li et al. (2006) results: FE simulation results (with Abaqus) are derived by those authors, considering an imposed relative density $\rho^* = 0.01$; the equivalent Poisson's ratio, the equivalent shear and traction moduli are given successively versus the material modulus by

$$\nu_{12} \approx 0.48; G_{12} = 3.2.10^{-5}E_s; E_1 = 9.61.10^{-5}E_s$$

3.2 Validation by comparison with analytical models and FE simulations

The results of homogenized properties (this work) are numerically compared with those available in the literature in Table 5, for a relative density $\rho^* = 0.01$[3] .

Equivalent properties	Zhu et al. (1997)	Homogenized properties (this work)	Li et al. (2006)	Gibson and Ashby (1997)
Young's modulus	$E_{100} = 9.94e - 5E_s$	$E_{100} = 9.94e - 5E_s$	$E_1 \approx 9.61e - 5E_s$	$E \approx 1e - 4E_s$
Poisson's coefficient	$\nu_{12} = 0.485$	$\nu_{12} = 0.485$	$\nu_{12} \approx 0.48$	$\nu \approx 0.33$

Table 5: Homogenized properties for "Tetrakaidecahedral" truss compared with literature values

---

[3]One has to take a small enough equivalent density to keep a large enough L/D ratio: a density 0.01 sets a length to width ratio of 4.

It is nevertheless acknowledged by several authors that Kelvin foams manifest a slight anisotropy (Zhu et al. (1997); Li et al. (2006);Warren and Kraynik (1997)); this is for instance noticed by Li et al. (2006), although not confirmed neither by experiments, nor by numerical simulations. Values of the Poisson coefficient predicted by Zhu et al. (1997) (~ 0.5) as well as by Li et al. (2006) (~ 0.48) are close to incompressibility, but do not really correspond to the observations on PU foams: according to Gibson and Ashby (1997), the value of Poisson's ratio ranges between 0.3 and 0.4 (0.33 in average). Nevertheless, the contraction effect shall decrease for strong compressions, according e.g. to Zhang and Lu (2007), who performed numerical simulations which sustain this behavior. According to Li et al. (2006), the contraction coefficient shall also decrease when the relative density increases. The smaller value observed in experiments must be due to other phenomena, in our opinion, such as a random variation of geometrical parameters, the collapse of beams, or additional uncontrolled phenomena occurring at the nodes.

4 Conclusions and perspectives

The discrete homogenization method based on asymptotic expansions of the fields (nodal position, forces and moments) proves as a systematic method to calculate the equivalent - in a homogenized sense - properties of lattices with a general periodic architecture (characterized by the topology of beams within a repetitive unit cell). The novelty of the present approach lies in the consideration of beam lattices and in the calculation of the transverse forces, which does not require the moment equilibrium, since the expression of the transverse forces is linked to the relative displacements of the extremities of a given beam, in the spirit of beam theory.

The situation of foams in their first elastic regime (small displacements) has been considered in this contribution, thereby excluding buckling, strain localization phenomena and inelastic deformations. The obtained effective properties are expressible as closed form expressions of the geometrical and mechanical parameters of the lattice microbeams. The present developments have been implemented in a software dedicated to the computation of homogenized properties of general 2D and 3D trusses in the geometrical linear framework. Applications to the calculation of the effective mechanical behavior of foams in 2D and 3D situations illustrate the versatility of the method, and its applicability to a wide range of architecture materials in a broad sense. Textiles are further architectured materials for which the present homogenization technique may be applicable, provided the interactions between structural micro-elements (the weft and warp yarns in the armor, which generate internal reactions due to their contact) are additionally incorporated.

Through the given applications and lattices considered in this work, the discrete homogenization technique has proven its ability to provide equivalent moduli in the elastic regime and in the linear geometrical framework for compression tests, which are in agreement with the equivalent properties obtained by parallel FE simulations.

A classification of lattices in terms with respect to rotations has been provided, highlighting the need to consider additional rotational degrees of freedom at both the micro and macroscale in a consistent manner. Accordingly, a micro-polar equivalent continuum model has to be adopted at the macroscale when micro-rotations of the node lattice are considered, as required in some loading cases. The extension of the asymptotic homogenization to micro-polar continua constitutes an important perspective of the present work. This extension, in addition to the derivation of the micropolar effects, will allow the treatment of special trusses (the chiral truss; trusses with negative Poisson's coefficients, such as inverted honeycombs). It is expected to provide results related to flexion or shear resistance versus the Young's modulus being different in comparison to a Cauchy continuum. These realizations open up from a general point of view the perspective of optimizing the topology and the mechanical properties of materials having a discrete structure such as foams, but also textiles or more generally any repetitive structure made of discrete elements akin to 1D structural elements like beams or beams.

Globally speaking, the discrete homogenization provides an explicit link between the micro and the macroscale behaviors, hence increasing our understanding of the microstructural origin of the deformation mechanisms of the architectured materials widely used nowadays.

References

Alkhader, M.; Vural, M.: Mechanical response of cellular solids: Role of cellular topology and microstructural irregularity. *International Journal of Engineering Science*, 46, (2008), 1035–1051.

Badiche, X.; Forest, S.; Guibert, T.; Bienvenu, Y.; Bartout, J.-D.; Ienny, P.; Croset, M.; Bernet, H.: Mechanical properties and non-homogeneous deformation of open-cell nickel foams: application of the mechanics of cellular solids and of porous materials. *Materials Science and Engineering*, A289, (2000), 276–288.

Burgardt, B.; Cartraud, P.: Continuum modeling of beamlike lattice trusses using averaging methods. *Computers and Structures*, 73, (1999), 267–279.

Caillerie, D.; Mourad, A.; Raoult, A.: Discrete homogenization in graphene sheet modeling. *Journal of Elasticity*, 84, (2006), 33–68.

Despois, J.-F.; Mueller, R.; Mortensen, A.: Uniaxial deformation of microcellular metals. *Acta Materialia*, 54, (2006), 4129–4142.

Gibson, L. J.: Biomechanics of cellular solids. *Journal of Biomechanics*, 38, (2005), 377–399.

Gibson, L. J.; Ashby, M. F.: *Cellular Solids*. Press syndicate of the university of Cambridge (1997).

Li, K.; Gao, X.-L.; Subhash, G.: Effects of cell shape and strut cross-sectional area variations on the elastic properties of three-dimensional open-cell foams. *Journal of the Mechanics and Physics of Solids*, 54, (2006), 783–806.

Mourad, A.: *Description topologique de l'architecture fibreuse et modelisation mecanique du myocarde*. Ph.D. thesis, I.N.P.L. Grenoble (2003).

Pedro, M. D.; Gmur, T.; Botsis, J.: *Introduction à la mécanique des solides et des structures*. presses polytechniques et universitaires romandes (2004).

Pradel, F.; Sab, K.: Cosserat modelling of elastic periodic lattice structures. *C. R. Acad. Sci. Paris,*, t. 326, Serie II b,, (1998), p. 699–704.

Raoult, A.; Caillerie, D.; Mourad, A.: Elastic lattices: equilibrium, invariant laws and homogenization. *Ann Univ Ferrara*, 54, (2008), 297–318.

Roberts, A.; Garboczi, E.: Elastic properties of model random three-dimensional open-cell solids. *Journal of the Mechanics and Physics of Solids*, 50, (2002), 33–55.

Sullivan, R. M.; Ghosn, L. J.; Lerch, B. A.: A general tetrakaidecahedron model for open-celled foams. *International Journal of Solids and Structures*, 45, (2008), 1754–1765.

Tollenaere, H.; Caillerie, D.: Continuous modeling of lattice structures by homogenization. *Advances in Engineering Software*, 29, (1998), 699–705.

Warren, W.; Kraynik, A.: Linear elastic behaviour of a low density kelvin foam with open-cell. *J. Appl. Mech.*, 64, (1997), 787–794.

Warren, W. E.; Byskov, E.: Three-fold symmetry restrictions on two-dimensional micropolar materials. *European Journal of Mechanics A/ Solids*, 21, (2002), 779–792.

Zhang, J.-L.; Lu, Z.-X.: Numerical modeling of the compression process of elastic open-cell foams. *Chinese Journal of Aeronautics*, 20, (2007), 215–222.

Zhu, H. X.; Knott, J. F.; Mills, N. J.: Analysis of the elastic properties of open-cell foams with tetrakaidecahedral cells. *J Mech. Phys. Solids.*, 45, (1997), 319–343.

Address: F. Dos Reis, J.F. Ganghoffer, LEMTA, ENSEM. 2, Avenue de la Foret de Haye. BP 160. 54504 Vandoeuvre Cedex. France
email: `jean-francois.ganghoffer@ensem.inpl-nancy.fr`;
`francisco.dos-reis@ac-strasbourg.fr`